A SYNOPSIS

Of the thesis

Synthesis and Characterization of Iron Oxide-based Nanomaterial and their Potential Applications

To be submitted

As a partial fulfilment for the award of the degree of

DOCTOR OF PHILOSOPHY

In

CHEMISTRY

By

Sanghavi Bindi Shashikantbhai

Under the supervision of

Dr. Hemant P. Soni

(Associate Professor)

Department of Chemistry,

Faculty of Science

The Maharaja Sayajirao University of Baroda

Vadodara 390002 India

November-2023

SYNOPSIS OF THE THESIS

To be submitted to **The Maharaja Sayajirao University of Baroda** for the award of the degree

DOCTOR OF PHILOSOPHY in Chemistry

Name of Student	:	**Sanghavi Bindi Shashikantbhai**
Title of the Thesis	:	**"Synthesis and Characterization of Iron Oxide-based Nanomaterial and their Potential Applications"**
Name of the Supervisor	:	**Dr. Hemant P Soni**
Faculty	:	**Faculty of Science, The Maharaja Sayajirao University of Baroda.**
Department	:	**Department of Chemistry**
Registration No	:	**FOS/2095**
Date of Registration	:	**7th March, 2018**

Sanghavi Bindi S.
Research Student

Dr. Hemant P. Soni
Research Guide

Prof. A. V. Bedekar
Offg. Head
Department of Chemistry

The synopsis of the thesis will be presented in the form of following chapters

Chapter 1	***Introduction***
Chapter 2	***Synthesis and Characterisation of Amino acid-capped transition metal ion-doped iron oxide nanoparticles***
Chapter 3	***Amino acid-capped transition metal ion-doped iron oxide nanoparticles: evaluating drug delivery carrier efficiency and in vitro magnetic resonance image contrasting ability***
Chapter 4	***Synthesis of Fe_3O_4 Nanoparticles Using Different Amino Acid Molecules as Templates, Their Characterization and Applications as Vehicle for Drug Delivery***
Chapter 5	***Fe_3O_4@L-Arginine and Fe_3O_4@L-Histidine Nanoparticles for One pot Solvent-free Sequential Knoevenagel-Michael Addition Reactions***

Chapter 1

Introduction

In the last century, materials science has attracted great interest in several areas of research due to their various application but with the introduction of nanotechnology, has raised more interest for scientific community due to their profound properties even a negligible functionalization of a nanomaterial brings about huge changes in its physical and chemical properties which can be obtained through different techniques, such as physical or chemical methods. Nanomaterials is wide class of material which deals with particles in the range of 1–100 nm which facilitate easy adsorption, absorption and penetration due to increased molecular interactions (Fig. 1).

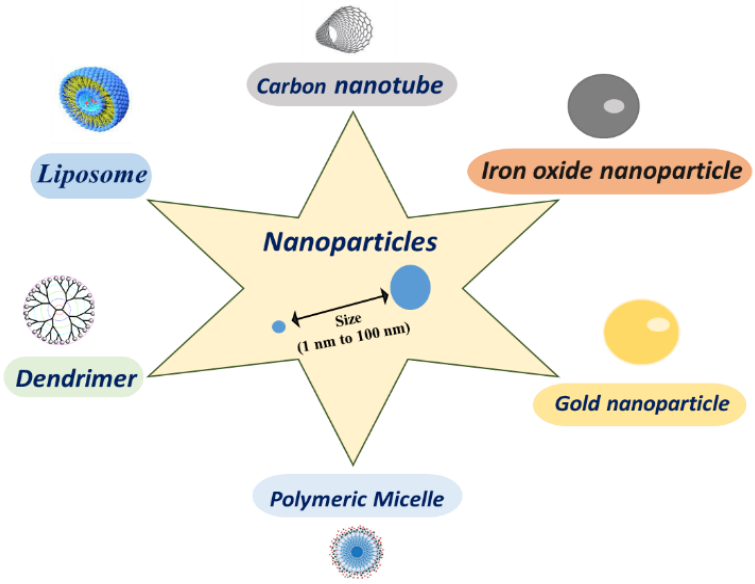

Fig. 1. Various types of nanoparticles based on their properties

Synthesized Nanomaterials can be varies from 0 to 3 dimensional which depends on the overall size and shape of materials [1-5].

Iron oxide (Fe_3O_4) capped amino acid nanoparticles:

Amino acids have outstanding biocompatibility and bonding surface chemistry with magnetic nanomaterials due to their functional groups (– COOH and -NH_2) which help to modify the morphology of nanoparticles [6-7].

Recently, magnetic nanomaterials capped with amino acids have been extensively utilized as solid supported heterogeneous catalysts due to their stability, selectivity, activity and recyclability.

Naturally available amino acids are good choice to work as a capping agent due to low cost, easily available and simply bonding with magnetic iron oxide nanoparticles (Fig. 2).

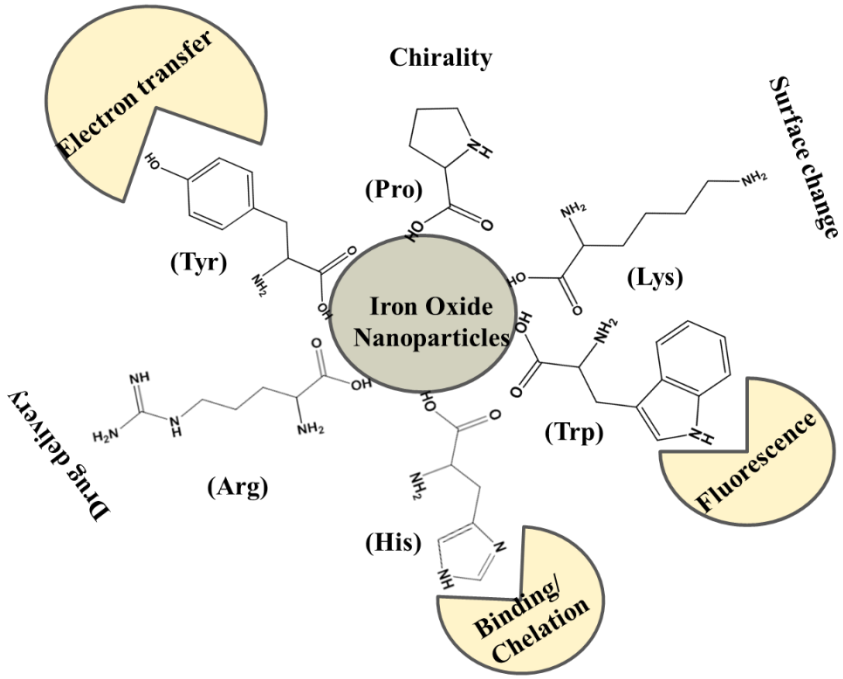

Fig. 2. Application of magnetic nanoparticles (Iron oxide) capped with amino acid molecules.

Nanocatalysts:

Nanoparticles (NPs) and materials like aluminium, iron, titanium dioxide, and silica all have been used as catalyst in nanoscale in organic and inorganic form in the past decades [8,9]. Along these lines, in this quest for eco-friendly and more affordable catalyst, nano-catalysis is rotating into a significant field in science, which is applied broadly in the academics and industrial areas (Fig. 3).

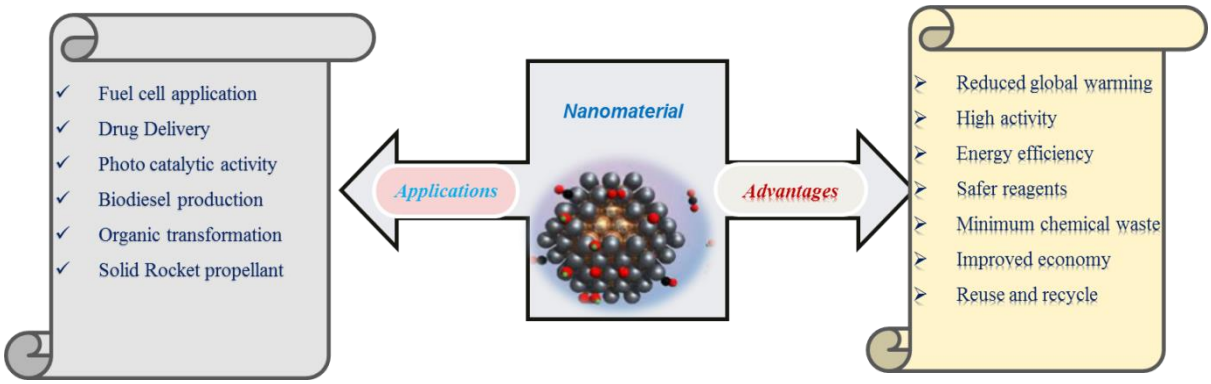

Fig. 3. Applications and advantages of nanocatalyst in various fields.

Magnetic Nanoparticles (Iron oxides) as a catalyst:

Nanoparticles having magnetic properties are of great interest for scientific community due to their low toxicity, superparamagnetic properties, such as surface area and volume ratio, and simple separation methodology, magnetic iron oxide (Fe_3O_4 and g-Fe_2O_3) NPs have attracted much attention and are particularly interesting in biomedical applications in heterogeneous and homogenous catalysis, biomedicine, magnetic fluids, data storage magnetic resonance imaging (MRI), and environmental remediation such as water decontamination [10-15]. In recent year, the role of magnetic nanoparticles in organic synthesis as heterogeneous catalyst is significantly increasing due to their high surface area, outstanding stability and recyclability (Fig. 4).

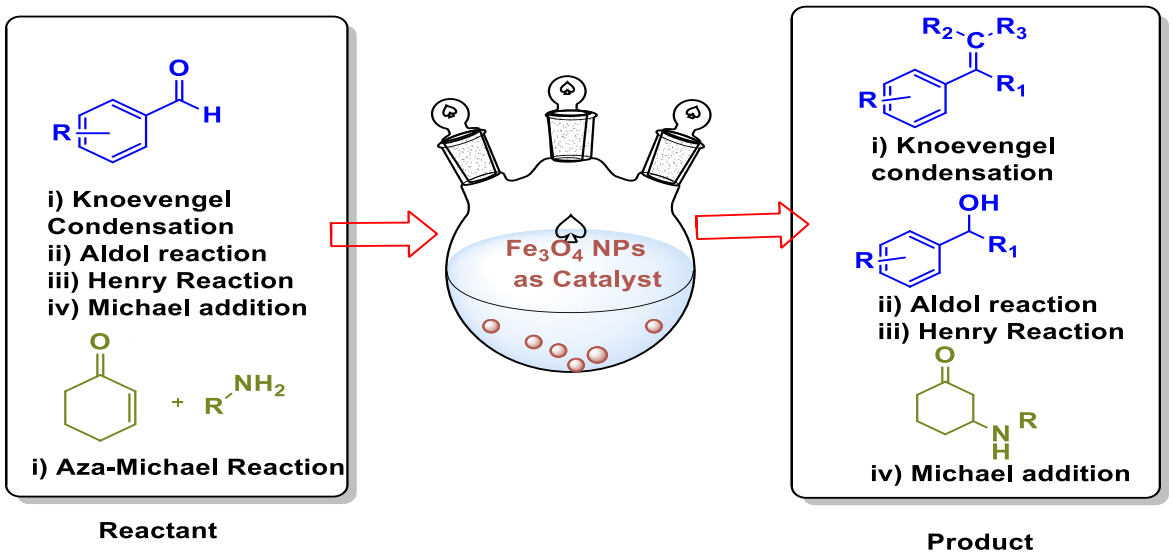

Fig. 4: Magnetic Nanoparticles (Iron oxide) as a catalyst in various organic transformation.

Iron Oxide Nanoparticles for Biologistic Activity

Various parts to developed magnetic iron oxide nanoparticles as a standard of biomedicinal materials and used these materials for biomedicinal applications such as drug delivery vehicles, MRI, gene delivery and cell labelling etc. Generally, magnetic iron oxide nanoparticles capped with amino acid have been established for therapy applications. Magnetic nanoparticles can be easily synthesized by wet chemical methods and then can be applied to various organic transformations.

With these views, we have synthesized and developed an iron oxied-based nanomaterials and their potensil application in various fileds and the contents of the present thesis are summarized in this abstract.

Chapter 2

Synthesis and Characterisation of Amino acid-capped transition metal ion-doped iron oxide nanoparticles

Introduction

The advantages of using magnetite for these applications are that it is non-toxic and decomposes into iron acting as an iron pool required for the synthesis of haemoglobin during erythropoiesis. In this study, we have synthesized Ultra-Small Iron Oxide NPs (Fe_3O_4-USIONs) and ferrites (MFe_2O_4) by a simple co-precipitation method. We focused on tuning the intrinsic magnetic property of USIONs by varying the transition metal dopant ions under the same reaction conditions rather than adopting the solvothermal or any other tedious synthesis methods. We report, here, the tuning of magnetism and improvement as well as the reversal of MR contrasting ability by doping Fe_3O_4 with suitable transition metal ions (Zn^{2+}, Mn^{2+}, and Ni^{2+}).

Experimental

Synthesis of L-arginine capped magnetic nanoparticles (Fe_3O_4@L-Arg NPs)

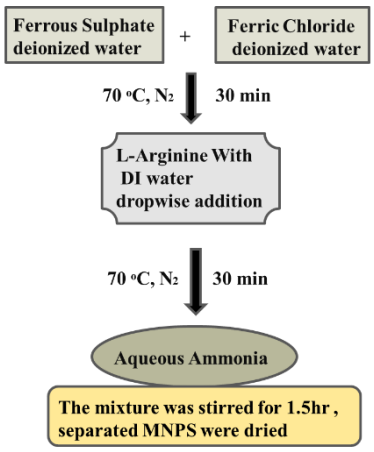

Synthesis of L-arginine capped transition metal ion doped magnetic nanoparticles (M^{+2}/Fe_3O_4@L-Arg NPs).

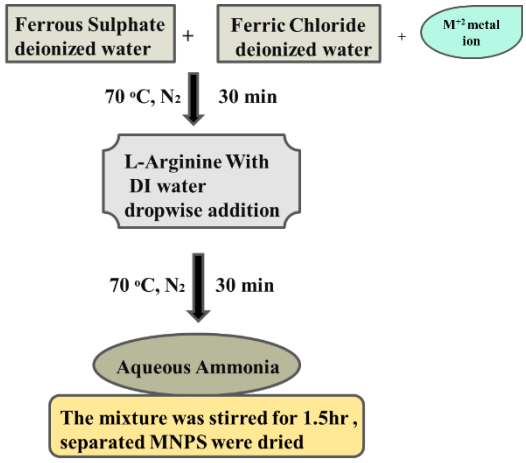

Synthesis of brigatinib-loaded Fe3O4@ L-Arg/P magnetic micelles (Fe_3O_4@L-Arg/P/bg)

Loading efficiency (%) = (Weight of drug loaded weight of total drug added) × 100

Drug loading% = (the mass of loaded drug/ the mass of initial drug and carrier) × 100

The drug loading efficiency and drug loading percentages were **64.0** and **8.35%,** respectively.

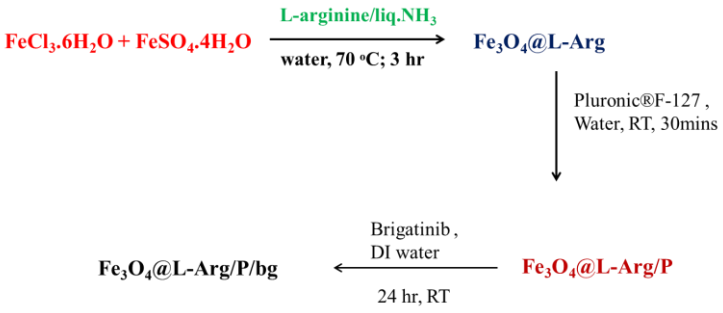

Characterization

Infrared Spectroscopy

The mode of interaction of L-arginine with the surface Fe ions of Fe3O4 NPs was studied by using Fourier Transform Infrared Spectroscopy.

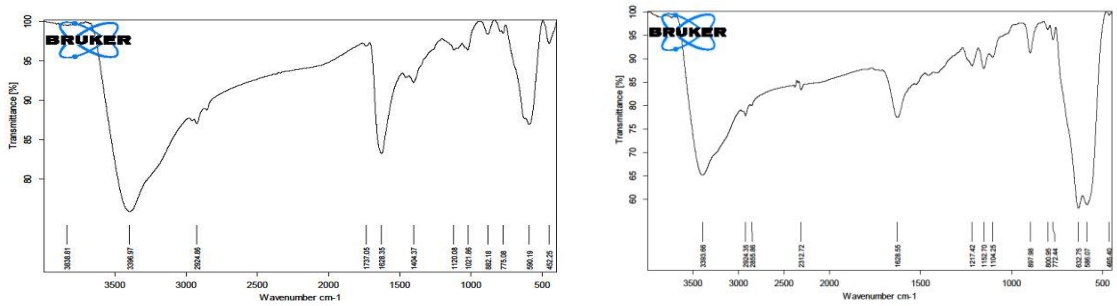

Fig. 5. FTIR Spectra of as-synthesized Fe3O4@L-Arg and Fe3O4@L-Arg/P

The interaction of L-arginine with Fe3O4 NPs surface was studied by FTIR spectroscopy. Free carboxylate ions in acetate form vibrate in two fundamental modes: asymmetric vas(COO–) and symmetric vs (COO–) stretching at 1583and 1422 cm−1, respectively.

XRD pattern

XRD patterns of Fe_3O_4 nanoparticles. Its phase is **inverse spinel** structure in which oxygen forms FCC arrangement and Fe cations occupy the interstitial Td or Oh sites. Using Debye Scherrer formula crystallite size 56 nm was obtained.

Fig. 6. XRD patterns of Fe3O4 nanoparticles

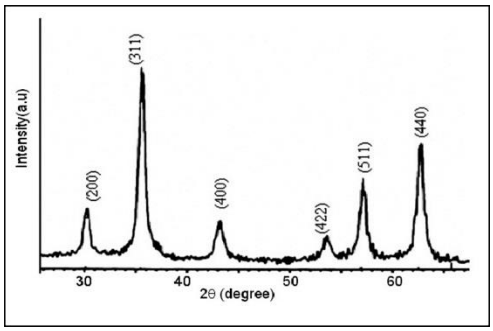

Fig.7. XRD pattern of the as-synthe M2+/Fe3O4@L-Arg nanoparticles

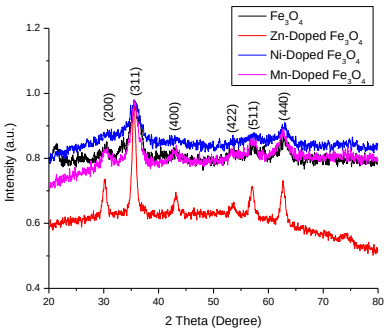

From the XRD pattern it can be observed that dopant ions do not affect the phase purity of the material or induce any strain. The diffraction peaks at 2ϑ values 30.1, 35.25, 43.15, 53.67, 57.32, and 63.16 correspond to (200), (311), (400), (422), (511) and (440) planes (JCPDS 82-1533), respectively.

High-Resolution Transmission Electron Microscopy (HRTEM) analysis

The morphology of the samples was examined by Transmission Electron Microscopy (TEM, Philips Tecnai 20) at 200 kV. All measurements were taken at 25 °C in deionized water. Further, the size and shape of M^{2+}/Fe_3O_4@L-Arg/P NPs were studied by High-Resolution Transmission Electron Microscopy (HRTEM)

analysis. The HRTEM images show spherical particles, and the size histograms reveal 10–12 nm particle size. The SAED patterns show the polycrystalline nature of the material.

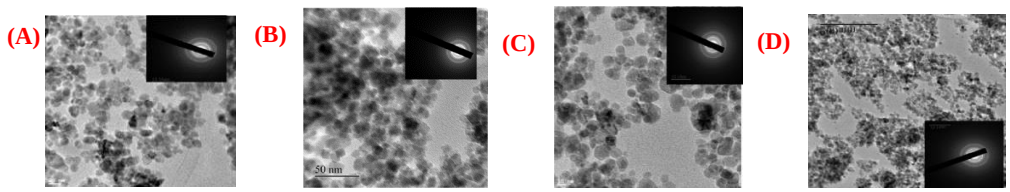

Fig. 8. **A–D** HRTEM images (inset image shows SAED pattern)

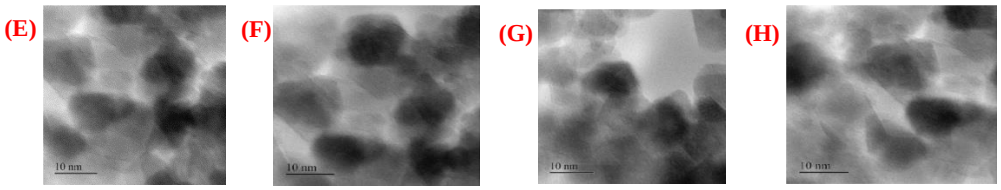

Fig. 9. E–H HRTEM lattice fringes at higher magnification of as-synthesized blank, Zn2+, Mn2+, and Ni2+/ Fe3O4@L-Arg/P NPs, respectively

VSM analysis

VSM analysis

The effect of doping on the magnetic propert the material was studied by VSM analysis. From the M-H curves, it can be observed that Fe3O4 NPs exhibit paramagnetic behaviour with less Ms value (30.1 emu/g), while on doping, it increases to 72.5 emu/g. Generally, in the bulk form, blank Fe3O4 has a Ms value of 80–90 emu/g and it increases upon transforming into a nanoregime.

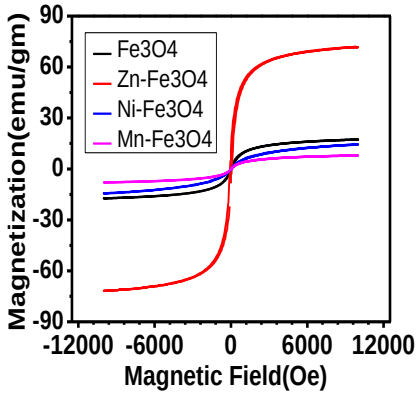

Fig. 10. VSM analysis for as-synthesized materi

Thermal analysis

Moreover, the successful encapsulation of surfaces by the Pluronic-F127 layer was confirmed by the thermal analyses. To evaluate the presence of inner sphere H-bonded water in the shell environment, a thermal analysis of all the samples was carried out.

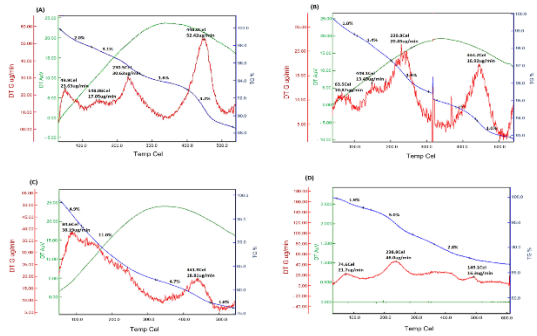

Fig. 11. Thermal analysis of (**A)** Fe_3O_4@ L-Arg/ Ni^{2+}/ Fe_3O_4@L-Arg/P (**C)** Mn^{2+}/ Fe_3O_4@L-Arg/P (**D)** Zn^{2+}/ Fe_3O_4@L-Arg/P NPs

Chapter 3

Amino acid-capped transition metal ion-doped iron oxide nanoparticles: evaluating drug delivery carrier efficiency and in vitro magnetic resonance image contrasting ability

Introduction

Very few iron oxide-based MRI CAs are available in the market globally (e.g., Ferridex®, Endorem®, and Resovist®) as compared to Gd-based CAs, even though there is an abundance of research reported in this area. The main reasons are i) Their physical properties vary with particle size, and ii) The uniform particle size (monodispersity) of the suspension is crucial. We report, here, the tuning of magnetism and improvement as well as the reversal of contrasting ability by doping Fe3O4 with suitable transition metal ions (Zn2, Mn2+, and Ni2+). We have demonstrated by in vitro studies that doped magnetite shows higher drug delivery efficiency with improved performance as MRI CAs.

In vitro drug release kinetics

To study the drug release kinetics, three different experiments were performed. This study was carried out at 37 °C and pH 7.4. In each experiment, 3.0 mg of brigatinib loaded magnetic NPs was added to a flask having 30 mL of Na_2HPO_4–NaH_2PO_4 buffer solution.

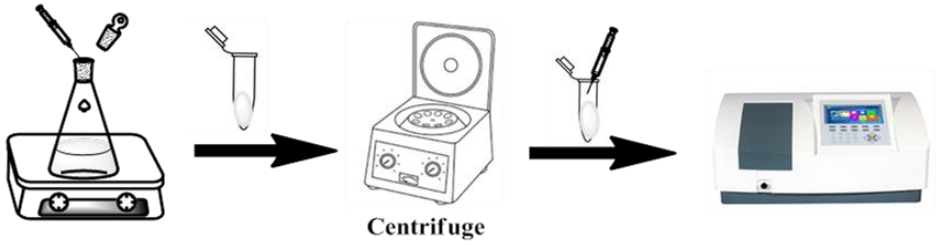

In vitro drug release kinetics, cell viability and cytotoxicity studies

The M^{2+}/Fe_3O_4@L-Arg/P NPs were tested as drug delivery vehicles for the epidermoid carcinoma cell line A431 to evaluate the anti-cancer activity of the loaded drug (Brigatinib). The smooth release, cytotoxicity, and colony-forming ability of these formulations were checked by the drug release kinetics, MTT, and clonogenic assays, respectively.

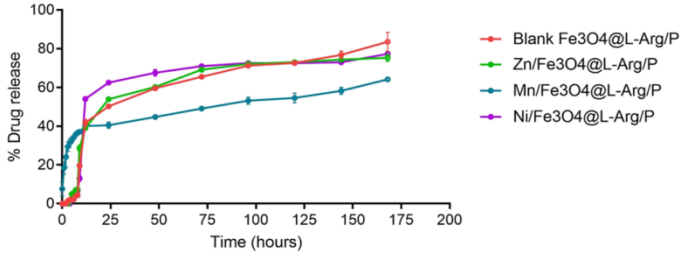

Fig. 11 Percentage release of brigatinib from Zn^{2+}, Mn^{2+}, and Ni^{2+}- doped Fe_3O_4@ L-Arg/P/b drug released from Mn^{2+}- Doped Fe_3O_4 Arg/P/bg is the earliest as compared to o However, at the end of three days (72 h), mor is released from Zn^{2+} and Ni^{2+}- doped USION Mn^{2+}-doped ones

Clonogenic Assay

We used a clonogenic assay to determine the colony-forming ability of cells under the effect of different treatments. The *in vitro* cell survival assay is based on the ability of a single cell to grow into a colony. It is generally carried out to determine the effect of a drug on the proliferation of tumor cells.

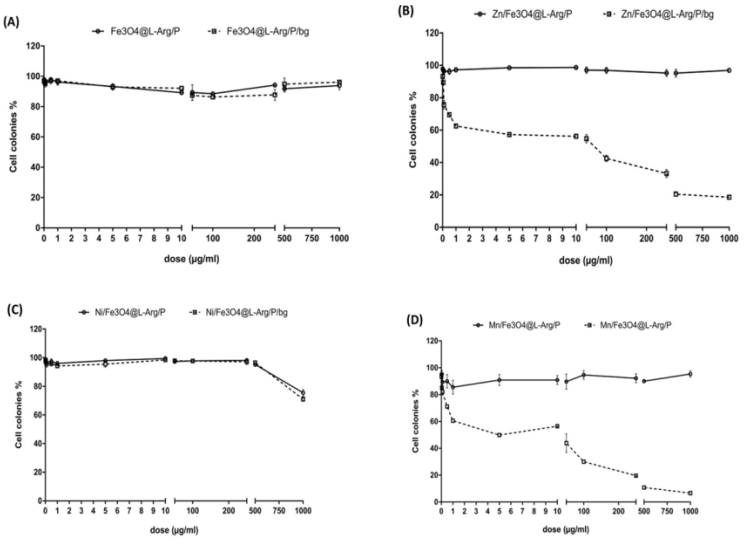

Fig. 12. Clonogenic assay: **A** No visible char the plates was observed in presence of the bared drug at any concentration (in µg level number of colonies remained constant throughout **B** colony formation reduced early at 1 µg mL−1 of the Zn2+/Fe3O Arg/P/bg. **C** No change in the number of col on the addition of Ni2+/Fe3O4@L-Arg/P/bg. The reduction in the number of colonies obs above 500 µg mL−1 dose. **D** The colony formation drastically decrease µg mL−1 dose of Mn2+/ Fe3O4@L-Arg formulation.

Phantom study

The correlation between T1 and T2 relaxation rates (R1 or R2) and the concentration of CAs can be investigated through the phantom study. The sequences of the radio frequency signal repetition time (TR) and the detection or echo time (TE) were designed such that the T1-weighted and T2-weighted images of the cross section of a capillary containing the sample in a coronal mode can be captured in an MRI machine.

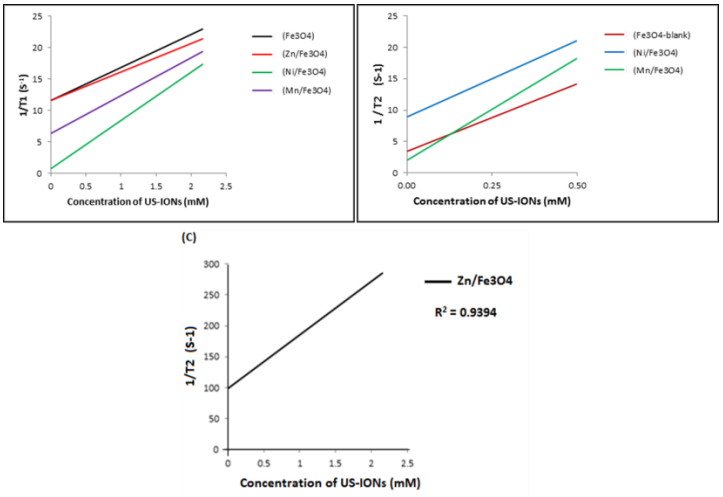

Fig. 13. A 1/*T*1 **B** and **C** 1/*T*2 Vs concentration of M2+/ Fe3O4@L-Arg/P NPs

Discussion

The commercially available Gd-DTPA and Gd-DOTA complexes have their ninth valence satisfied by a water molecule (q = 1). There is a very small energy difference between their eighth and ninth valence. From a three-dimensional perspective, there can also be a faster water exchange between these surface-ligand-bound H-bonded water molecules and those of the bulk water molecules through diffusion. In this way, the τM parameter can be controlled. The advantage of this strategy is that the number of inner spheres water molecules (q) will be more than one and this high number will collectively make the electronic relaxation time (Tie) longer. Overall, high proton relaxivity can be achieved by tuning both the core and the shell environment in the developed USIONs (Scheme 2).

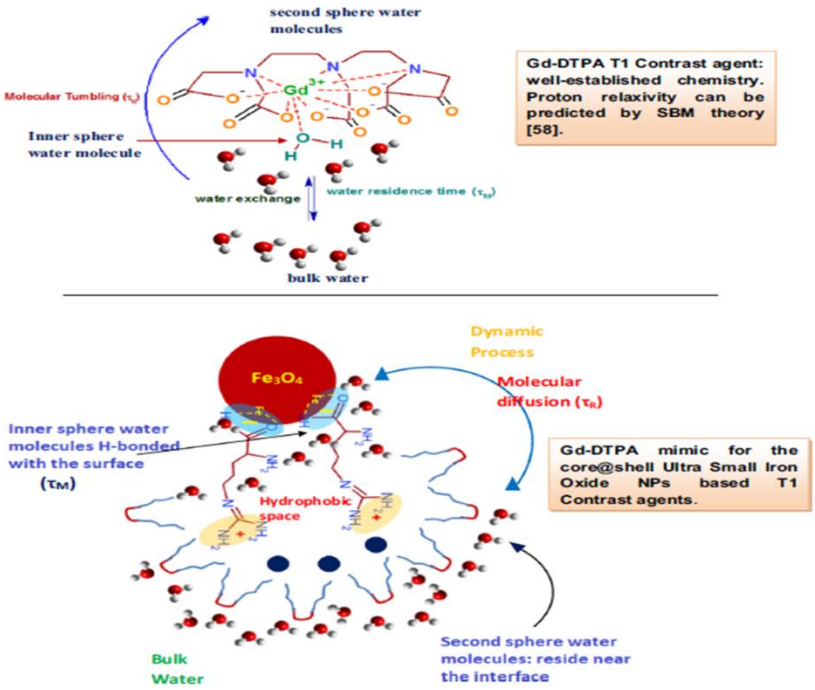

Scheme 1: The upper panel shows standard Gd-DTPA chemistry from SBM theory. The lower panel shows the proposed Gd-DTPA mimic based on the proposed tuning of the core@shell environment of USIONs

Conclusion

Small amino acid molecules like L-arginine can act as capping and chelating ligands to bind Fe_3O_4 Nanoparticles tightly, restrict their growth at the Nano regime, and form USIONs. Pluronic F127 encapsulates L-Arg capped USIONs effectively and forms polymeric micelles while retaining magnetic properties. The synthesized Pluronic-encapsulated and L-Arg-capped Fe_3O_4 magnetic micelles can act as drug delivery platforms to load the hydrophobic anti-cancer drug brigatinib in their hydrophobic shells.

Chapter-4

Synthesis of Fe_3O_4 Nanoparticles Using Different Amino Acid Molecules as Templates, Their Characterization and Applications as Vehicle for Drug Delivery

Introduction

SPIONs can perform this job very well because of the strategy of extending their time at the target site through controlled release of a predetermined amount of the drug while monitoring disease abatement progress. The idea behind using Fe_3O_4 as a vehicle to load brigatinib and target cancer cell as follows .

Experimental

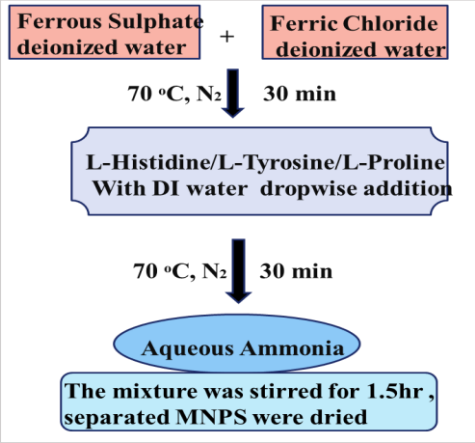

Fig. 4.3. Synthesis of brigatinib loaded Fe_3O_4@L-AA/P magnetic micelles.

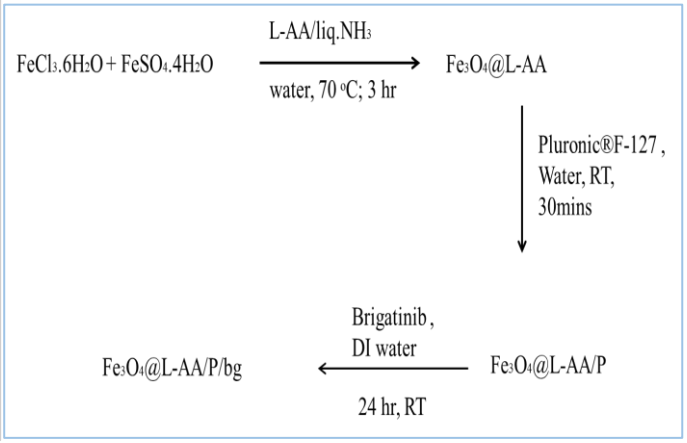

Scheme 4.1. Synthesis of brigatinib loaded Fe_3O_4@ L AA/P magnetic micelles (Fe_3O_4@L AA/P/bg).

Loading efficiency (%) = (Weight of drug-loaded/weight of total drug added) x 100…….. (1)

Drug loading percentage = The mass of loaded drug/the mass of initial drug and carrier x 100….(2)

The drug loading efficiency and drug loading percentage were found to be 40.56 and 10.52% respectively.

In vitro drug release kinetics, cell viability and cytotoxicity studies

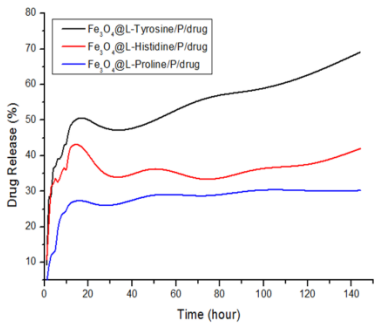

Fig. 4.11. Percentage release of brigatinib from Fe_3O_4@ L-AA/P/bg.

The drug released Fe_3O_4@ L-pro/P/bg is the earliest as compared to others. However, at the end of three days (72 h), more drug is released from Fe_3O_4@ L-Tyr/P/bg and Fe_3O_4@ L-His/P/bg than Fe_3O_4@ L-pro/P/bg ones.

In vitro drug release kinetics

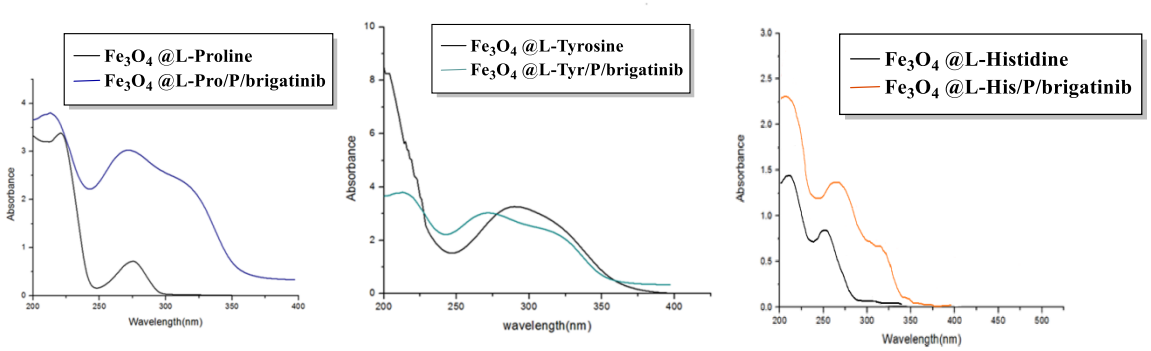

Fig. 4.12. UV-vis studies for control release of brigatinib for as synthesized Fe_3O_4/L-AA/P NPs.

In Vitro Cytotoxicity Assay

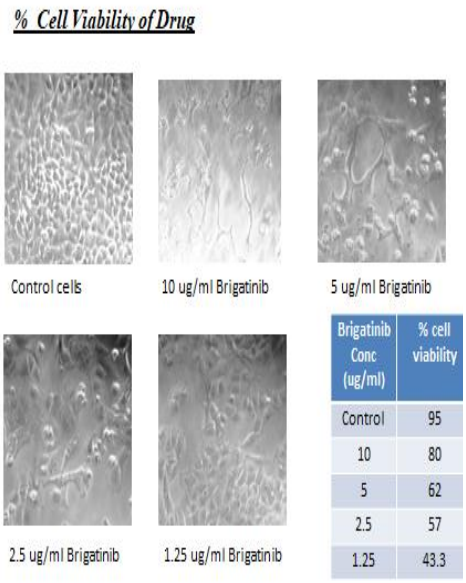

Brigatinib Conc (ug/ml)	% cell viability
Control	95
10	80
5	62
2.5	57
1.25	43.3

Fig. 4.14. Cytotoxicity studies of the dru as-synthesized Fe_3O_4 nanoparticles.

In the present work, we have reported the synthesis of iron oxide nanoparticles using three amino acids (AA-L-Tyrosine, L-Proline and L-Histidine) as a capping agent. Pluronic- F127, a surfactant triblock co-polymer, was used to encapsulate the AA/Fe_3O_4 NPs. The resulting magnetic micelles, with AA capped Fe_3O_4 NPs as the core and the pluronic surfactant as the shell, were transfected into a human bone marrow MCF7 and A549 cell-lines *in vitro* to evaluate cell death.

MTT Assay

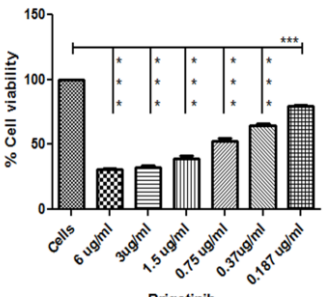

The cytotoxic effect of the synthesized USIONs with or without the drug was studied by MTT assay, on the MCF47 and A549 for human breast cancer and lung cancer cell lines, respectively

Fig. 4.15. MTT Assay on Drug (brigatinib).

Conclusion

From this study, it can be concluded that: (i) drug can makes stable bonding with nanoparticles on its surface by intermolecular H-bonding or by entrapping inside cavities; (ii) pluronic like copolymeric surfactant which are capable to acquire 'mild' positive charge in the intra cellular environment can provide stealth and flexible surface to the delivery vehicle. More experiments are needed to establish this claim for eukaryotic cells in a large scale. Hence, iron oxide nanoparticles can serve as non-toxic, biodegradable and safe vectors to load a variety of drug/gene of useful products like enzymes, proteins, peptides, hormones etc into the cells. Such a carrier can also be used for delivering genes into eukaryotic cells and can be a potential candidate for use in gene therapy also.

Chapter 5

Fe_3O_4@L-Arginine and Fe_3O_4@L-Histidine Nanoparticles for One pot Solvent-free Sequential Knoevenagel-Michael Addition Reactions

Introduction

Multicomponent reactions involving heterogeneous catalysis in organic synthesis have advantages over enzyme/homogeneous catalysis like superior atom economy, atom utilization, and selectivity can be achieved with savings in cost, energy, and time. In attempts to develop green synthesis protocols and COP-MCRs, we explored here, the tandem Knoevenagel-Michael addition reactions at a single catalytic site leading to the products having a tri-substituted C-C bond in the molecular framework.

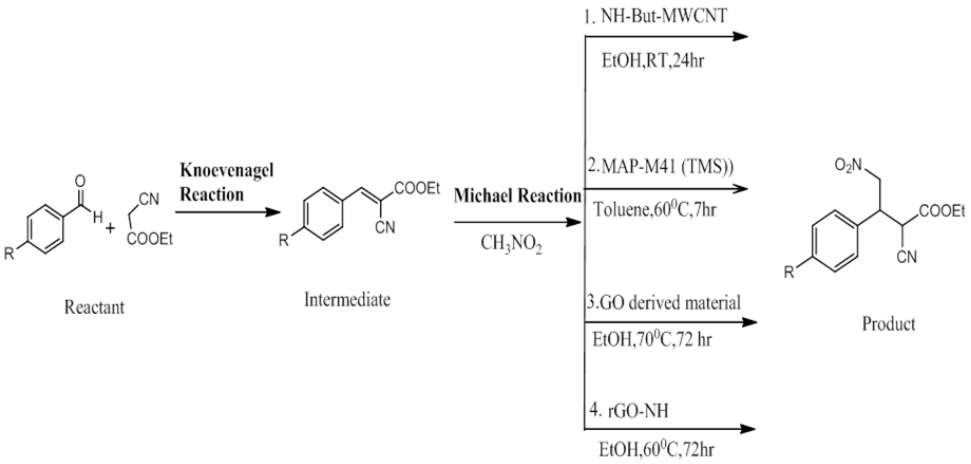

In the present work, we have carried out one-pot KMS of different aromatic aldehydes under solvent-free conditions in the presence of as-synthesized catalysts leading to precursors of the above-discussed drug molecules. We achieved high reaction yield and conversion in a short time. The catalysts were easily isolated from the reaction mixture and recycled effectively for up to five cycles.

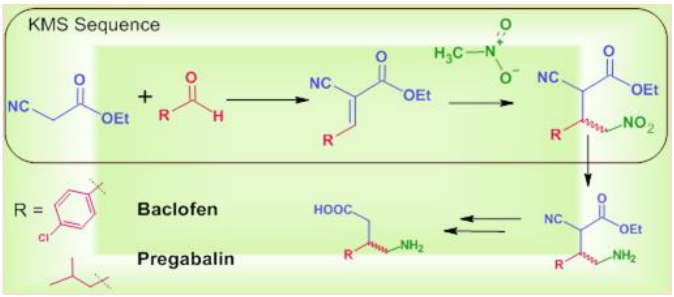

Scheme 2. Synthesis scheme involving KMS sequence leading towards pharmaceutically important drugs.

Experimental

Fig. 14. Synthesis of Fe_3O_4@AANPs

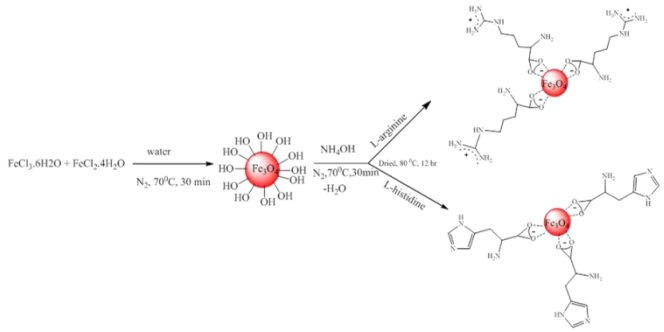

Characterization of synthesized Catalysts by following methods

i)PXRD, ii) FESEM, iii) TEM,
iv) FTIR v) VSM, vi) TGA
vii) UV-visible viii) BET analysis

Results and Discussion

- General procedure for sequential Knoevenagel and Michael addition reaction

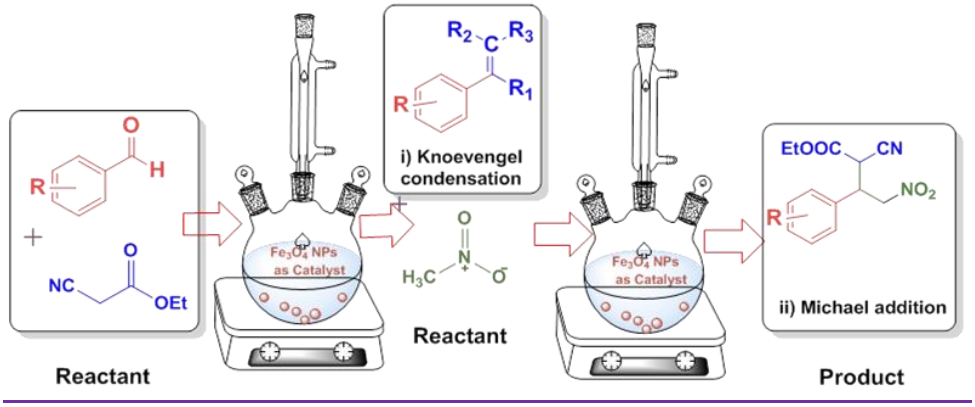

Optimization of reaction parameters for model Knoevenagel condensation reaction

For optimizing the reaction parameters, the model Knoevenagel reaction was carried out under different sets of conditions concerning different catalysts, amount of Fe_3O_0@L-Arg and Fe_3O_4@L-Hist, solvents, and temperature.

Table 1. Knoevenagel condensation reaction between aromatic/aliphatic aldehydes and ethyl cyanoacetate catalyzed by Fe_3O_4@L-Arg and Fe_3O_4@L-Hist NPs.[a]

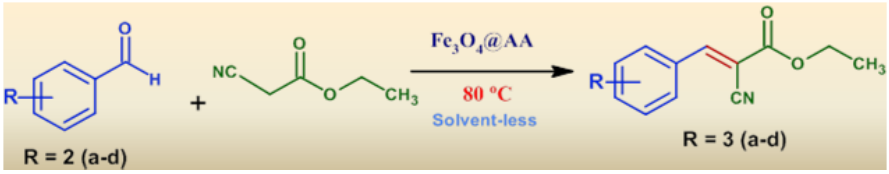

Aldehyde	Product	Time (min)		%Yield[b,c]	
		Fe_3O_4@L-Hist	Fe_3O_4@L-Arg	Fe_3O_4@L-Hist	Fe_3O_4@L-Arg
(1a)	(2a)	180	150	91	94
(1b)	(2b)	75	50	94	97
(1c)	(2c)	180	150	89	90
(1d)	(2d)	180	150	87	89
(1e)	(2e)	90	75	92	95
(1f)	(2f)	90	70	91	93
(1g)	(2g)	90	73	90	91
(1h)	-------	180	150	--	--
(1i)	-------	180	150	--	--

Table 2. Fe_3O_4@L-Arg catalyzed sequential Michael addition reaction with Knoevenagel condensation product.

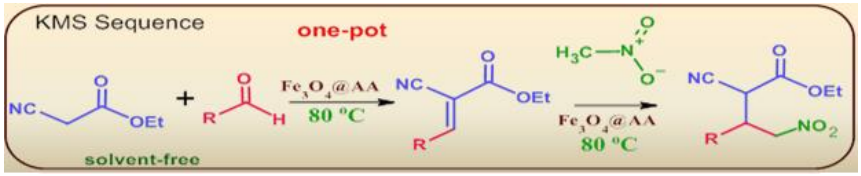

Knoevenagel Adduct	Product	Time (h)	%Yield[b]	
			Fe_3O_4@L-Hist	Fe_3O_4@L-Arg
(2a)	(3a)	6	--	69
(2b)	(3b)	5	--	72
(2c)	(3c)	5	--	70
(2d)	(3d)	6	--	67

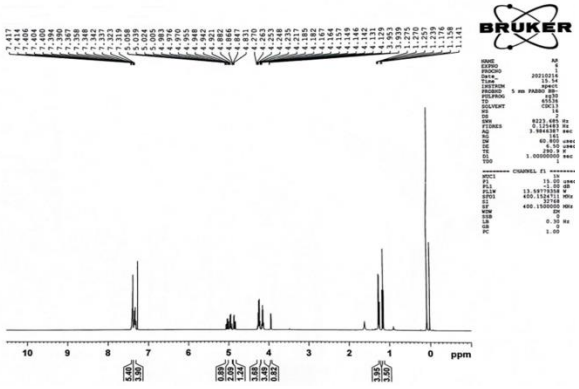

Recovery and recycling of Fe_3O_4@L-Arginine and Fe_3O_4@L-Histidine NPs and Proposed mechanism

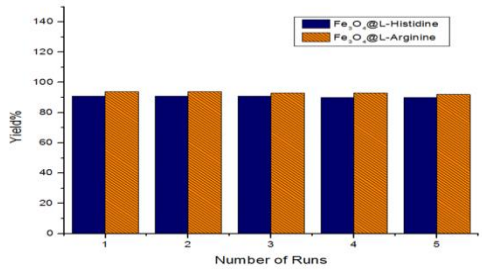

Fig. 15. Recovery and recycling study of Fe_3O_4@L-Arg and Fe_3O_4@L-HistNPs for Knoevenagel reaction.

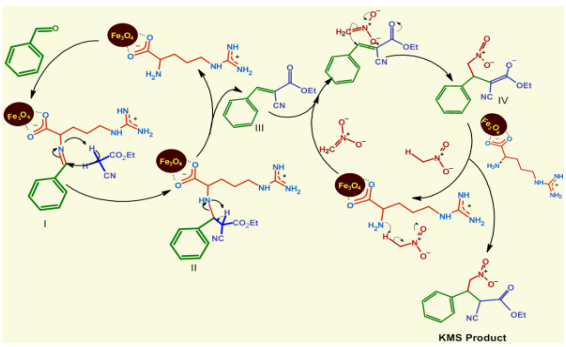

Scheme 3. Proposed mechanism for KMS in the presence of Fe_3O_4@L-Arg NPs

Origin of Reactivity

It can be observed that the Fe_3O_4@L-Arg NPs show higher catalytic activity than the Fe_3O_4@L-Hist NPs in the case of the Knoevenagel reaction due to the effective delocalization of side chain guanidine nitrogen's positive charge and flexibility of the adsorbed amino acid molecular framework on the surface of Fe3O4 nanoparticle.

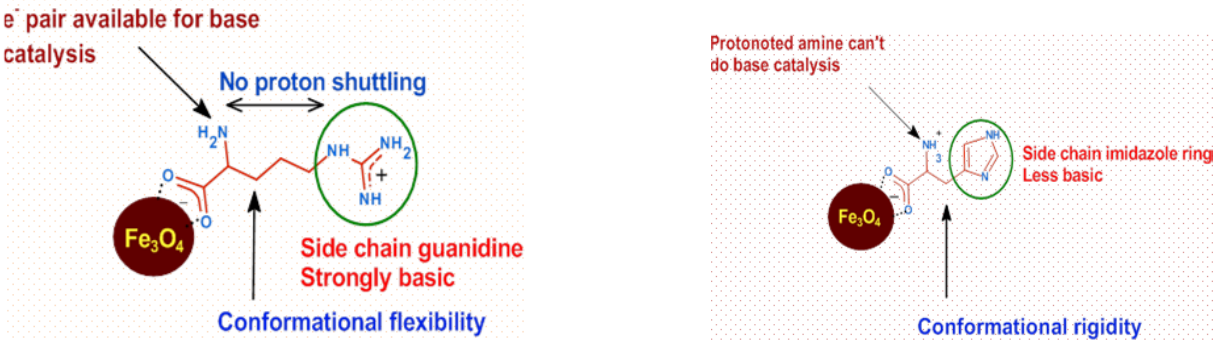

Fig. 16. Origin of difference in reactivity of Fe_3O_4@L-Arg and Fe_3O_4@L-Hist NPs catalytic systems.

Conclusion

The developed process becomes more cost-effective than those based on bare noble metal catalysts catalyst recovery is made simple by using a magnetic field. The catalyst Fe_3O_4@L-Arg is more effective than Fe_3O_4@L-Hist for both sequential reactions. The reaction is "green" because no hazardous solvents are used, and the entire one-pot process can be carried out in solvent-free conditions with short reaction times, high product yields, and high activity and stability of the catalyst under the optimized reaction conditions.

References

1. Duran N, Mattoso LHC, Morais PC (2006) Nanotecnologia: introdução, preparação e caracterização de nanomateriais e exemplos de aplicação. São Paulo: Artliber. Fernandes MTC, Garcia RBR, Leite CAP
2. Srivastava M, Chaubey A, Ojha AK (2009) Investigation on size dependent structural and magnetic behavior of nickel ferrite nanoparticles prepared by sol-gel and hydrothermal methods. Mater Chem Phys 118(1):174-180.
3. Yetter AR, Risha GA, Son SA (2009) Metal particle combustion and nanotechnology. P Combust Inst 32(2):1819-1838.
4. Tiwari, J.N., Tiwari, R.N., Kim, K.S., 2012. Zero-dimensional, one dimensional, two-dimensional and three-dimensional nanostructured materials for advanced electrochemical energy devices. Prog. Mater Sci. 57, 724–803.
5. Laurent, S., Forge, D., Port, M., Roch, A., Robic, C., Vander Elst , L., Muller, R.N., 2010. Magnetic iron oxide nanoparticles: synthesis, stabilization, vectorization, physicochemical characterizations, and biological applications. Chem. Rev. 110. , pp. 2574–2574.

6. Nosrati H, Salehiabar M, Bagheri Z et al (2018) Preparation, characterization, and evaluation of amino acid modified magnetic nanoparticles: drug delivery and MRI contrast agent applications. Pharm Dev Technol 23:1156–1167.

7. S.L. Candelaria, Y. Shao, W. Zhou, X. Li, J. Xiao, J.-G. Zhang, Y. Wang, J. Liu, J. Li, G. Cao,Nanostructured carbon for energy storage and conversion, Nano energy, 1 (2012) 195-220.

8. K. Yan, A. Chen, Efficient hydrogenation of biomass-derived furfural and levulinic acid on the facilely synthesized noble-metal-free Cu–Cr catalyst, Energy, 58 (2013) 357-363.

9. K. Nanthagopal, B. Ashok, A. Tamilarasu, A. Johny, A. Mohan, Influence on the effect of zinc oxide and titanium dioxide nanoparticles as an additive with Calophyllum inophyllum methyl ester in a CI engine, Energy Convers. Manag. 146 (2017) (2017) 8–19.

10. B. Ashok, K. Nanthagopal, A. Mohan, A. Johny, A. Tamilarasu, Comparative analysis on the effect of zinc oxide and ethanox as additives with biodiesel in CI engine, Energy 140 (P1) (2017a) 352–364.

11. 16. K. Nanthagopal, R.S. Kishna, A.E. Atabani, A.H. Al-Muhtaseb, G. Kumar, A. Ashok, Compressive review on the effects of alcohols and nanoparticles as an oxygenated enhancer in compression ignition engine, Energy Convers. Manag. 203 (2020) 112244.

12. 17. B. Ashok, K. Nanthagopal, A.K. Jeevanantham, P. Bhowmick, D. Malhotra, P. Agarwal, An assessment of calophyllum inophyllum biodiesel fuelled diesel engine characteristics using novel antioxidant additives, Energy Convers. Manag. 148 (15) (2017) 935–939.

13. 18. P. Senthilkumar, S. Rashmitha, P. Veera, C.V. Ignatious, C. SaiPriya, A.V. Samrot, Antibacterial activity of neem extract and its green synthesized silver nanoparticles against Pseudomonas aeruginosa, Pure Applied Microbiol. 12 (2018),02.

14. A.V. Samrot, N. Shobana, Rashmi Jenna, Antibacterial and antioxidant activity of different staged ripened fruit of Capsicum annuum and its green synthesized silver nanoparticles, Bionanoscience 8 (2018a) 632–646.

15. A.V. Samrot, P. Raji, A.J. Selvarani, P. Nishanthini, Antibacterial activity of some edible fruits and its green synthesized silver nanoparticles against uropathogen –Pseudomonas aeruginosa SU 18, Biocatal. Agricult. Biotechnol. 16 (2018b)253–270.

Sanghavi Bindi S.
Research Student

Dr. Hemant P. Soni
Research Guide

Prof. A. V. Bedekar
Offg. Head
Department of Chemistry